Seismic expression of shear zones: Insights from 2-D point-spread-function based convolution modelling

T. Wrona [a,b,*], H. Fossen [c], I. Lecomte [a], C.H. Eide [a], R.L. Gawthorpe [a]

[a] Department of Earth Science, University of Bergen, Allégaten 41, N-5007, Bergen, Norway
[b] Helmholtz Centre Potsdam, GFZ German Research Centre for Geosciences, Telegrafenberg, 14473, Potsdam, Germany
[c] Museum of Natural History, University of Bergen, Allégaten 41, N-5007, Bergen, Norway

ABSTRACT

Shear zones are common strain localization structures in the middle and lower crust and play a major role during orogeny, transcurrent movements and rifting alike. Our understanding of crustal deformation depends on our ability to recognize and map shear zones in the subsurface, yet the exact signatures of shear zones in seismic reflection data are not well constrained. To advance our understanding, we simulate how three outcrop examples of shear zones (Holsnøy - Norway, Cap de Creus - Spain, Borborema - Brazil) would look in different types of seismic reflection data using 2-D point-spread-function (PSF)-based convolution modelling, where PSF is the elementary response of diffraction points in seismic imaging. We explore how geological properties (e.g. shear zone size and dip) and imaging effects (e.g. frequency, resolution, illumination) control the seismic signatures of shear zones. Our models show three consistent seismic characteristics of shear zones: (1) multiple, inclined reflections, (2) converging reflections, and (3) cross-cutting reflections that can help interpreters recognize these structures with confidence.

1. Introduction

Shear zones (i.e. tabular volumes of rock with higher strain than the surrounding rocks) play an important role in accommodating tectonic deformation in the crust and mantle (e.g. Vauchez et al., 2012; Snyder and Kjarsgaard, 2013). As shear zones generally form in the ductile mid-to-lower crust, they are less often exposed at the surface than brittle faults. Geophysical techniques, such as 2-D and 3-D seismic reflection data can help us image and study shear zones in the subsurface (e.g. Clerc et al., 2015; Phillips et al., 2016; Lenhart et al., 2019). Since strain variations often correlate with physical property changes (e.g. density and seismic velocity), we expect shear zones to appear on seismic reflection data, and in rare cases surface outcrops of exhumed shear zones can be directly correlated with reflection patterns in seismic images (e.g. Fossen and Hurich, 2005). Nevertheless, the characteristic seismic signatures of shear zones are still poorly constrained, particularly in the common case where shear zones form anastomosing zones or networks. Understanding seismic signatures of shear zones is critical to recognize and quantify strain in continental rifts and margins.

Moreover, we could use 2-D and 3-D seismic reflection data to study the spatial and temporal evolution of shear zones. Once mapped, we can measure geometric shear zone properties (e.g. orientation, thickness, length), which help us understand the growth and interaction of these structures (see review by Fossen and Cavalcante, 2017). Unravelling the

evolution of shear zones also helps us quantify and understand the distribution/localization of strain within the lithosphere (e.g. Duretz et al., 2014; Kiss et al., 2019). To support these studies, we investigate the seismic signatures of shear zones using 2-D point-spread function (PSF) based convolution modelling.

Seismic modelling techniquesincluding convolution simulate the seismic response of geological structures (e.g. Lecomte et al., 2015). As such, these techniques are forward solutions to the inverse problem of seismic interpretation, i.e. explaining the observed seismic image with a reasonable geological model. Seismic modelling by convolution is often preferred because it is highly efficient, flexible and easy to use, yet in its simplest 1-D approach it only gives a good estimate of the vertical seismic resolution, as a series of synthetic seismic traces generated by convolving reflectivity logs with a wavelet are aligned to generate a synthetic (pseudo) 2-D seismic section (e.g. Osagiede et al., 2014; Jafarian et al., 2018). This approach is neither accounting for lateral resolution effects, as the trace spacing (sometimes combined with smoothing) sets an arbitrary lateral resolution, nor for illumination effects, as even extremely steep reflectors can be imaged with sufficiently close trace spacing.

To include both the effects of lateral resolution and limited illumination of steep dips, we use true 2-D convolution modelling (Lecomte et al., 2016), i.e., applying a 2-D convolution operator (the point-spread function or PSF) directly to the entire 2-D reflectivity model. The

---

* Corresponding author. Department of Earth Science, University of Bergen, Allégaten 41, N-5007, Bergen, Norway.
  E-mail address: wrona@gfz-potsdam.de (T. Wrona).

Table 1

Geometric properties of shear zones: [1]Johnston et al. (2007), [2]Fossen (2010), [3]Milnes et al. (1997), [4]Norton (1986), [5]Fossen and Hurich (2005), [6]Wennberg et al. (1998), [7]Austrheim (1990), [8]Boundy et al. (1992), [9]Phillips et al. (2016), [10]Carreras (2001), [11]Younes and McClay (2002), [12]Koehn et al. (2015), [13]Salomon et al. (2015), [14]Goscombe and Gray (2008), [15]Goscombe et al. (2003), [16]Passchier et al. (2002), [17]Foster et al. (2009), [18]de Castro et al. (2012), [19]de Castro et al. (2008), [20]Kirkpatrick et al. (2013), [21]Neves and Mariano (1999), [22]Gontijo-Pascutti et al. (2010), and [23]Klepeis et al. (1999).

Location	Shear zone name	Thickness	Length	Displacement	Dip	Dip direction
W Norway	Nordfjord-Sogn	2–6 km[1]	120 km[2]	>50 km[3]	30–40°[4]	W[2]
SW Norway, North Sea	Hardangerfjord	5–6 km[5]	>600 km[5]	10–15 km[5]	22–23°[5]	NW[5]
W Norway	Bergen Arc	2–3 km[6]	50 km[6]	>14 km[6]	steep[6]	SW[6]
W Norway	Holsnøy	30–150 m[7]	>10 km[7]	–		N[8]
SW Norway, North Sea	Stavanger	1–2 km[9]	>200 km[9]	–	15–30°[9]	W[9]
NW Spain	Cap de Creus	20–300 m[10]	>10 km[10]	–	–	NNE-SSW[10]
Egypt	Rihba	>200 m[11]	~100 km[11]	–	–	–
Uganda, DR Congo	Nyamwamba		~50 km[12]	–	–	–
NW Namibia	Purros	1–5 km[13−15]	620 km[13−15]	–	70–90°, 30–50°, subvertical[13,16]	WSW to WNW, W[13,16]
NW Namibia	Three Palms	1–2 km[13]	>300 km[13]	–	60–90°, 40–55°, 10–65°[13,14,17]	W, E, W[13,14,17]
NE Brazil	Brasiliano	hundreds of metres to kilometres[18−20]	hundreds of kilometres[18−20]	–	subvertical18	–
NE Brazil	Borborema	2–5 km[21]	700 km[21]	~11 km[21]	≥65°[21]	NW,SE[21]
Southeast Brazil	Arcadia-Areal21	0.5–1 km[22]	~700 km[22]	–	30–80°[22]	–
New Zealand	Anita	3.5–4 km[23]	–	–	subvertical[23]	–

resulting 2-D seismic images correspond to pre-stack depth-migration (PSDM) seismic reflection data, because PSFs are diffraction-point responses of a PSDM imaging system describing how much distortion we expect going from reflectivity to seismic images (Lecomte, 2008). As such, the PSF contains: (1) the 1-D wavelet (i.e. frequency bandwidth), (2) the velocity, (3) the incident angle (including offset-dependent effects), and (4) illumination patterns. The illumination pattern determines which parts of a geological structure are imaged while also controlling the lateral resolution (Lecomte et al., 2016). The illumination pattern determines which parts of a geological structure are imaged (steeply-inclined reflectors are often poorly imaged in seismic reflection data) while also controlling the lateral resolution (Lecomte et al., 2016; Eide et al., 2018).

To investigate how shear zones look in seismic reflection data, we simulate the seismic signatures of three excellent outcrop areas using 2-D PSF based convolution modelling. These three shear zone networks were mapped in great detail (meter scale) over vast areas (several square kilometres) in: (1) Holsnøy (W Norway), (2) Cap de Creus (NE Spain), and (3) Borborema Province (NE Brazil). Our models highlight that the seismic signatures of shear zones depend on the complex interaction of a variety of geological and geophysical factors. Nevertheless, we are able to consistently identify three characteristic features of shear zones in our models: (1) multiple, inclined reflections, (2) converging reflections, and (3) cross-cutting reflections. We find that shear zones become difficult to identify when their dip is steeper than the illumination of the survey or when noise becomes >50%. Finally, we find that the geometric curvature of shear zones is a useful kinematic indicator, as seismic reflections forming an acute angle with the edge of the shear zone indicate movement towards the junction of reflections. These results will help identifying and mapping shear zones in 2-D and 3-D seismic reflection data, and help us understand the way strain is distributed in the ductile middle and lower crust in different tectonic settings.

2. Outcrop examples

We simulate the seismic signatures of three excellent outcrop examples of shear zone networks from (1) Holsnøy (Norway), (2) Cap de Creus (Spain), and (3) Borborema Province (Brazil). We chose these out of a large number of shear zones (Table 1), because they were mapped at high resolution (meter scale) over large areas (several square kilometres) using detailed field observations (Boundy et al., 1992; Austrheim et al., 1997; Neves and Mariano, 1999; Carreras, 2001).

2.1. Holsnøy (Norway)

On Holsnøy (an island in western Norway) a network of eclogitized shear zones are exposed in a thrust sheet in the Caledonian orogenic belt (Austrheim et al., 1997) (Fig. 1a). Geochronological data (423 ± 4 Ma U/Pb age) and field relations indicate that eclogitization and shear deformation of lower crustal Proterozoic granulites occurred during the Caledonian orogeny (Bingen et al., 2004). As the eclogization occurred under very high pressures (~2 GPa) and temperatures (700–750 °C) (Austrheim and Griffin, 1985; Raimbourg et al., 2005), it is clear that these shear zones formed at sub-crustal depths in lower crustal rocks during continental subduction. Post-orogenic collapse, extension, and erosion exposed these eclogites on the island of Holsnøy (Austrheim et al., 1997).

At present day, these shear zones are exposed over an area of approximately 36 km² (Fig. 1b). Shear zone widths vary from 30 to 150 m in a continuous anastomosing pattern (Austrheim, 1990; Boundy et al., 1992). While the shear zones consist of eclogite facies rocks (omphacite + garnet + kyanite + epidote + phengite + quartz ± amphibole ± plagioclase), the host rocks are mainly granulite facies mafic rocks (plagioclase + diopside + garnet ± scapolite ± orthopyroxene ± hornblende) (Austrheim and Griffin, 1985). The eclogite shear zones formed by fluid-assisted deformation that developed from initial fractures through shear zones to massive eclogite breccias carrying blocks of granulites in foliated eclogite (Austrheim et al., 1997; Raimbourg et al., 2005).

To build geological (reflectivity) models necessary for seismic modelling, we used physical measurements of these rocks available at present day (Austrheim, 1987; Austrheim et al., 1997) combined with an empirical relationship converting P- to S-wave velocities for granulite facies rocks and eclogites (Manghnani and Ramananantoandro, 1974) (Table 2). We consider these surficial properties to be sufficiently representative of the properties of the shear zone and host rock encountered at depth for the purpose of our study.

2.2. Cap de creus (Spain)

On the Cap de Creus peninsula in northeast Spain, a Variscan shear belt exposes an extensive network of ductile shear zones (Carreras, 2001) (Fig. 1b). Although a subject of debate, these shear zones probably developed during progressive wrench-dominated deformation in the Variscan. As a result, they formed under retrograde metamorphic
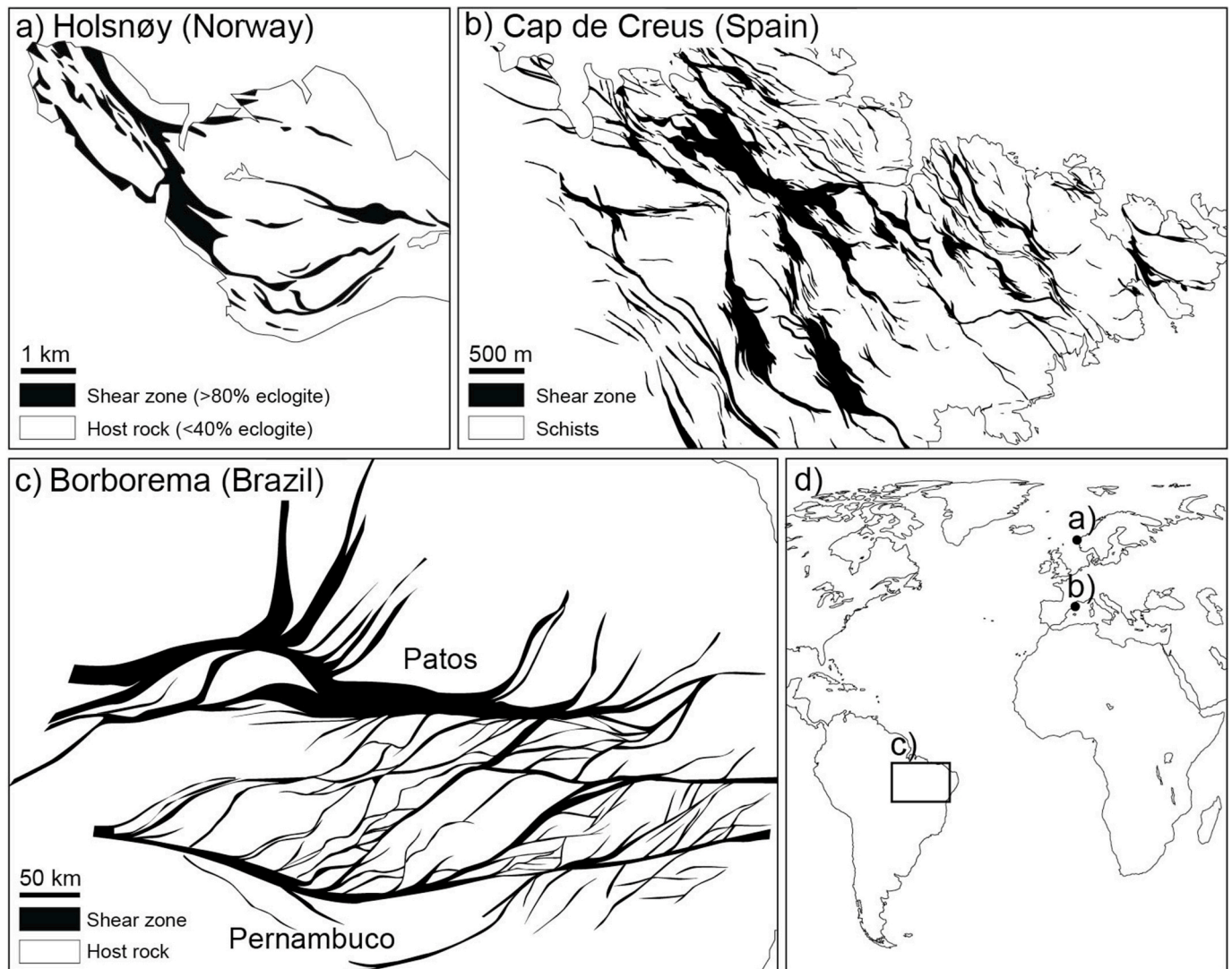
Fig. 1. Outcrop examples of shear zones from: a) Holsnøy, Norway (Boundy et al., 1992; Austrheim et al., 1997); b) Cap de Creus, NE Spain (Carreras, 2001), and c) Borborema, Brazil (Neves and Mariano, 1999). While the Holsnøy and Cap de Creus shear zones were mapped with field observations, mapping of the Borborema shear zone was assisted by magnetic data.

Table 2

Physical rock properties used for seismic forward modelling based on: [1]Empirical relation ($v_p \rightarrow \rho$) for mid to lower crustal rocks by Godfrey et al. (1997); [2]Measurement of five mylonites by Mainprice and Casey (1990); [3]Measurement of three schists by Godfrey et al. (2000); [4]Bulk density measurements by Austrheim (1987); [5]P-wave velocity measurements by Austrheim et al. (1997); [6]Empirical relation ($v_p \rightarrow v_S$) for granulate facies rocks and eclogites by Manghnani and Ramananantoandro (1974); [7]Typical physical properties of granites by Bourbié et al. (1987).

Location	Rocks	Bulk density [g/cm³]			P-wave velocity [m/s]			S-wave velocity [m/s]		
		Min	Max	Avg	Min	Max	Avg	Min	Max	Avg
Cap de Creus	Shear zone (Mylonite)	2.86[1]	2.95[1]	2.91[1]	5.60[2]	6.70[2]	6.15[2]	4.60[2]	3.80[2]	4.20[2]
	Host rock (Schist)	2.66[3]	2.72[3]	2.69[3]	5.60[3]	6.60[3]	6.10[3]	3.08[3]	3.51[3]	3.30[3]
Holsnøy	Shear zone (Eclogite)	3.06[4]	3.33[4]	3.19[4]	8.30[5]	8.50[5]	8.40[5]	3.95[6]	4,33[6]	4,14[6]
	Host rock (Granulite)	2.79[4]	3.21[4]	3.02[4]	7.50[5]	7.80[5]	7.65[5]	3,58[6]	4,16[6]	3,90[6]
Borborema	Shear zones (Mylonite)	2.86[1]	2.95[1]	2.91[1]	5.60[2]	6.70[2]	6.15[2]	4.60[2]	3.80[2]	4.20[2]
	Host rock (Granite)	2.50[7]	2.70[7]	2.60[7]	4.50[7]	6.00[7]	5.25[7]	2.50[7]	3.30[7]	2.90[7]

conditions in crystalline rocks with a pre-existing foliation. At present day, we can observe these shear zones over an area of ~20 km² (Fig. 1b). Shear zone widths reach values of up to 300 m in continuous anastomosing patterns predominantly in crystalline schists (Carreras, 2001). Neither surficial nor subsurface physical properties of these rocks are available, so we rely on physical properties typical for these rock types as represented by five mylonites (Mainprice and Casey, 1990) and three schists (Godfrey et al., 2000). These properties were combined with an empirical relationship converting P-wave velocity to density for mid to lower crustal rocks (Godfrey et al., 1997) to constrain the bulk density, P-wave velocity, and S-wave velocity of the geological model (Table 2).
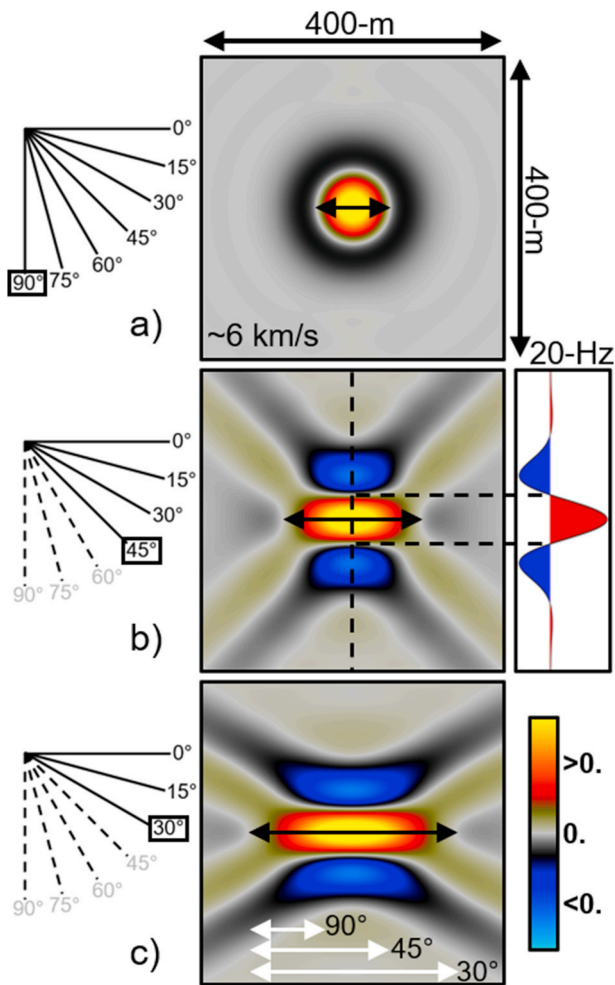
Fig. 2. Limited dip-illumination impact on lateral resolution as seen on 2-D Point-Spread Function for Cap de Creus, i.e., with about 6 km/s in average velocity and a 20-Hz Ricker wavelet. In the following, the resolution values are estimated at the nearest zero crossings around the central peak of the PSF. a) [0°-90°] dip-illumination case (perfect) resulting in a point-wise PSF with equal vertical and lateral resolution of about a quarter-of-a-wavelength (here about 75 m; horizontal black double arrow across PSF's peak); b) [0°-45°] dip-illumination case and corresponding lateral resolution (black double arrow), showing also the central trace with its Ricker-wavelet shape; c) [0°-30°] dip-illumination case with comparison (white double arrows at bottom) of the lateral resolution variations between a), b) and c).

2.3. Borborema Province (Brazil)

The Borborema Province (northeast Brazil) hosts a network of larger and smaller shear zones, of which the largest ones reach more than 20 km in width (Patos shear zone). Of the three shear zones that we model in this work, the Patos is the largest by an order of magnitude (to allow any comparison to seismic studies, we scaled down its length and width by a factor of 50). The shear zones are late Neoproterozoic and related to the Brasiliano orogenic system (Neves and Mariano, 1999; de Araujo et al., 2014) (Fig. 1c). Kinematic and geochronological data indicate that the shear zone network formed during overall dextral strike-slip shearing in a transpressional setting at around 580-570 Ma (Archanjo et al., 2002; de Araujo et al., 2014). This shear zone network covers almost the entire northeastern part of Brazil (Fig. 1c) and is considered to have continued on the African side prior to the South Atlantic break-up.

To our knowledge, relevant petrophysical measurements of these rocks are not available. We thus use empirical relationships to derive the

bulk density, P-wave velocity, and S-wave velocity for the relevant rock types, i.e. mylonites (Mainprice and Casey, 1990) and granites (Bourbié et al., 1987) combined with an empirical relation converting P-wave velocity to density for mid to lower crustal rocks (Godfrey et al., 1997) (Table 2). Note that, while we aim to constrain these properties as well as possible, they may still differ from the original rock properties, simply because it is not possible to include all geological structures (e.g. mesoscale and microscale fabrics and lithological variations) in these models.

2.4. Rotation

To compare shear zones from outcrop to seismic observations, it is necessary to convert these outcrop examples from map to cross-section view. While we typically interpret shear zones in 2-D or 3-D seismic images (Phillips et al., 2016; Fazlikhani et al., 2017; Clerc et al., 2018), the best outcrop examples of shear zones are exposed in map-view (Austrheim et al., 1997; Neves and Mariano, 1999; Carreras, 2001). To generate comparable seismic images of these shear zones, we need to rotate these outcrop examples from map to cross-section view. For the Holsnøy case, this is a matter of restoration to the original orientation of the shear zone network, which can be assumed to have been more horizontal-based on the regional tilting of all units in the area (e.g. Fossen, 1993). For the Cap de Creus and Borborema cases, the shear zones developed in a strike-slip dominated setting, and rotation is not justified by their geological history. However, these and previous studies of shear zones show no systematic difference between tectonic regime and network geometry; geometric differences are rather controlled by rheological variations, flow vorticity and strain (e.g. Gapais et al., 1987; Fossen and Cavalcante, 2017) in addition to rheological heterogeneities in the initial rocks.

3. Point-spread-function based convolution modelling

Generally, seismic images depend on the complex interaction of a large number of geological and geophysical factors (e.g. Yilmaz and Doherty, 1987; Sheriff and Geldart, 1995). This study focuses on the effects of two geological factors (aspect ratio and dip of the shear zone) as well as two geophysical factors (seismic frequency and illumination). Overall, seismic resolution is primarily a function of frequency bandwidth of the signal, host rock velocity, and the incident angle. The vertical seismic resolution (tuning thickness) is typically estimated as a fraction (e.g. a quarter) of the wavelength of the signal (Brown, 2011). While the lateral seismic resolution also depends on the wavelength, it is further limited by the illumination pattern (Lecomte et al., 2016) (Fig. 2). For perfect illumination (i.e. imaging of scattering structures from all directions; reflectors and diffractors alike), the lateral resolution is equal to the vertical one, as illustrated by the PSF itself which is diagnostic of the overall seismic imaging system, as it would be for any optical system such as cameras, microscopes, telescopes, etc (Fig. 2; Lecomte, 2008). Reflectors are then just dense sets of diffractors which might act in a coherent manner when properly illuminated, i.e. specular reflection, so knowing the elementary response of a diffraction point is sufficient information about any imaging system, according to Huygens' principle. In practice, limited illumination in seismic imaging results in a much lower lateral resolution than the vertical one for the illumination structures (Fig. 2b, c). Limited survey aperture, i.e., due to acquisition at the Earth's surface and within a certain area, further constrained by wave propagation issues such as ray path refraction, low signal energy due geometrical spreading and various sources of attenuations (scattering and anelasticity), and finally processing/imaging choices (e.g. migration aperture), all indeed concurred to reducing the illumination cone as illustrated in Eide et al. (2018) for imaging of volcanic intrusions, for example. Including illumination effects is therefore critical to seismic modelling, because it incorporates two common and important effects of seismic imaging especially at greater depths: (1) that
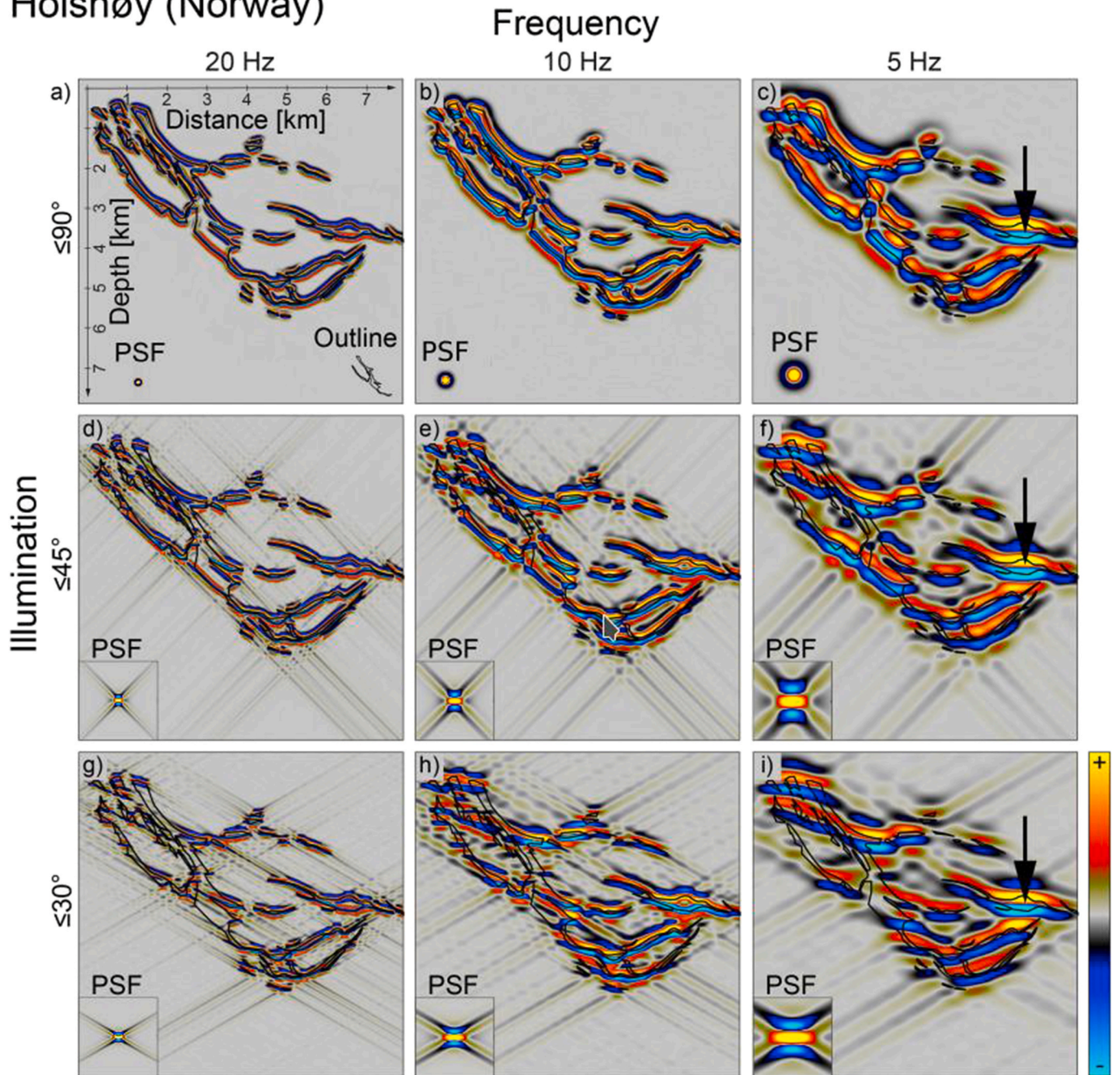
Fig. 3. Seismic signature of Holsnøy shear zone (Norway) in cross-section for different dominant frequencies (5, 10, 20 Hz) and maximum illumination angles (30°, 45°, 90°). The point-spread function (PSF) indicates the vertical and horizontal resolution of the seismic image. The seismic images correspond to zero-phase PSDM data. The colour bar is scaled to 50% of the maximum and minimum amplitudes. The black outline shows the shear zone geometry. Note how imaging quality decrease from the top left to the bottom right. The black arrows on c, f and i indicate amplitude anomalies arising from the termination of the reflection below. It is also worth noting that reflection curvature indicates the sense of movement of the shear zone.

interfaces dipping more steeply than a certain angle cannot be imaged, and (2) that lateral seismic resolution depends on the illumination pattern, i.e. seismic images are not solely impacted by vertical resolution issues.

For these reasons, we apply intrinsic 2-D PSF based convolution modelling to the outcrop examples described above. This technique allows us to generate 2-D PSDM seismic images of geological models including the key illumination and resolution effects mentioned above (Lecomte et al., 2015). Our workflow involves three steps. First, we extract reflectivity as a 2-D grid according to a selected incident angle

from the outcrop examples. Second, we generate the PSF using: (1) a Ricker wavelet (characterized by its dominant frequency), (2) an average velocity in the zone to image (Table 2), (3) an incident angle, and (4) a maximum reflector-dip angle to be illuminated. Third, a convolution between the PSF and the 2-D reflectivity grid produces the seismic images. We only use zero incident angle to simulate zero-offset acquisition, as even for large offsets at the surface incident angles become small for deep crustal shear zones (10–20 km). The maximum angle of reflector dip to be illuminated, which we just call '(maximum) illumination angle' in the following, describes that only reflectors
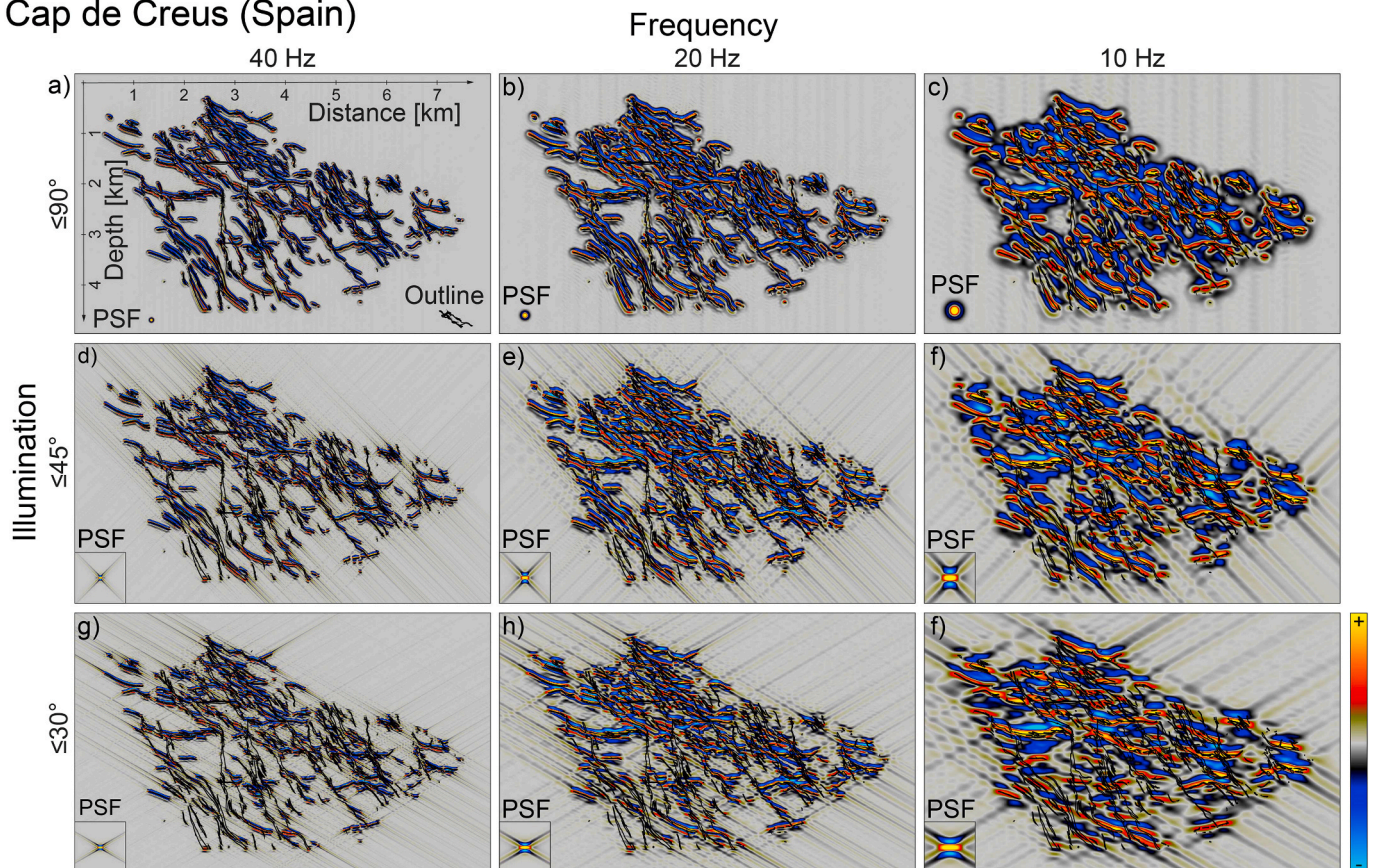
Fig. 4. Seismic images of the Cap de Creus shear zone (Spain) in cross-section for different dominant frequencies (10, 20, 40 Hz) and maximum illumination angles (30°, 45°, 90°). The point-spread function (PSF) indicates the vertical and horizontal resolution of the seismic image. The seismic images correspond to zero-phase PSDM data. The colour bar is scaled to 50% of the maximum and minimum amplitudes. The black outline shows the shear zone geometry. Note how imaging quality decrease from the top left to the bottom right.

dipping below this angle will be visible on the seismic images while steeper reflectors will not appear per se, though might be indirectly detected as discontinuities and amplitude variations of the seismic signals. As illustrated in Fig. 2, this angle also affects the lateral resolution; a 45° as steepest dip angle will roughly correspond to about half a wavelength lateral resolution. To maintain generalisability, we use a generic illumination described in (Lecomte et al., 2016), i.e. for cases with no specific survey design or overburden model in mind.

3.1. Geophysical factors

First, we explore how seismic signatures of these shear zones change dependent on the dominant frequency and maximum illumination angle. For this purpose, we generate seismic images of these three shear zones ranging from high to low quality by systematically varying dominant frequencies (of Ricker wavelets) and maximum illumination angles (of the PSF) over a large range of values for each example. This means that we use maximum illumination angles varying from 30 to 45 to 90° and dominant frequencies varying from 5 to 10 to 20 Hz for Holsnøy (Fig. 3); from 10 to 20 to 40 Hz for Cap de Creus (Fig. 4), and from 5 to 10 to 15 Hz for the downscaled Borborema shear zone (Fig. 5). Typical seismic surveys reach illumination angles of 40°–50° (Eide et al., 2018). The frequencies we selected cover typical acquisition parameters of seismic reflection surveys for the considered depths (1, 2, 4 s TWT) (e.g. Osagiede et al., 2014) (Table 3). We also explore the effects of noise on the seismic signatures of shear zones by systematically varying the level of noise, testing no noise (0%), a case where a third of the amplitudes are noise (33%), equal signal-to-noise (50%), and a case of only noise (100%) (Fig. 6).

3.2. Geological factors

Next, we explore how the seismic signatures of these shear zones change in different geological settings. While many geological factors can affect the seismic signatures of shear zones, we focus on two parameters in this study: the aspect ratio (i.e. width to length) and dip of the shear zone. To explore the effects of these parameters, we run models with aspect ratios of 1:1, 1:2 and 2:1 (i.e. map view geometry compressed to half the original width and length, respectively), and rotated to dips of 0°, 30° and 60° (Figs. 7, 8, 9). These values cover typical shear zone sizes and dips observed in the field (Table 1). Maximum illumination angles are set to 45° and dominant frequencies to 10 Hz (Holsnøy), 20 Hz (Cap de Creus) and 10 Hz (Borborema) corresponding to moderate seismic imaging quality.

4. Results

4.1. Geophysical effects

Our first set of models explores how geophysical parameters impact the seismic signatures of shear zones. Our models show the seismic signatures of the Holsnøy, Cap de Creus, and Borborema shear zone networks for different frequencies (5–40 Hz) and maximum illumination angles (30°, 45°, 90°) (Figs. 3, 4, 5). At maximum frequency and full illumination (≤90°), we obtain accurate images of all shear zones with clearly separable seismic reflections of each high strain area (Figs. 3a, 4a and 5a). At intermediate frequency and full illumination, we start to lose some details, as reflections begin to merge vertically and horizontally
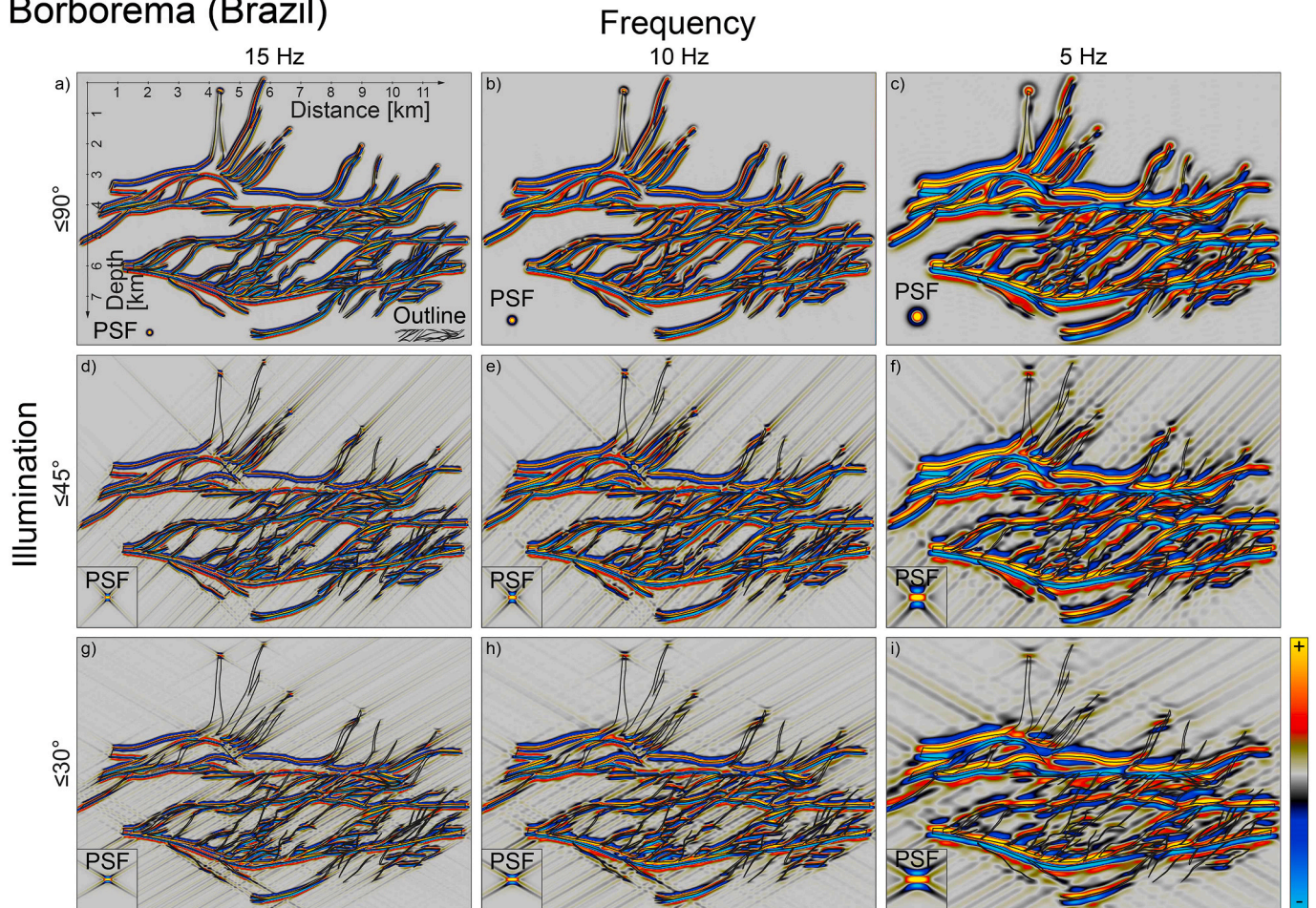
Borborema (Brazil)

Frequency

Fig. 5. Seismic images of the Borborema shear zone (Brazil) in cross-section for different dominant frequencies (5, 10, 15 Hz) and maximum illumination angles (30°, 45°, 90°). The point-spread function (PSF) indicates the vertical and horizontal resolution of the seismic image. The seismic images correspond to zero-phase PSDM data. The colour bar is scaled to 50% of the maximum and minimum amplitudes. The black outline shows the shear zone geometry. To compare the extremely-large Borborema shear zone to seismic studies, it was necessary to scale its length and width down by a factor 50. Note how imaging quality decrease from the top left to the bottom right. Moreover, it is worth noting that reflection curvature indicates the sense of movement of the shear zone.

(Figs. 3b, 4b and 5b), yet we are still able to observe the overall geometry of the shear zone. At low frequency and full illumination, we have lost most of the details: (1) thin reflections have disappeared, (2) closely spaced reflections merged, and (3) reflection terminations appear as amplitude anomalies (Figs. 3c, 4c and 5c). At this point, we can identify: (1) the overall shape, (2) orientation, and (3) some internal intersections of the shear zone. At intermediate illumination (≤45°), steeper geometries show lower amplitudes and fewer anomalies (Figs. 3d–f, 4d-f, 5d-f). This effect continues for limited illumination (≤30°), where inclined reflections disappear. At this stage, we can only see a few disjointed sub-horizontal reflections (Fig. 3g–i, 4g-i, 5g-i).

4.1.1. Seismic noise

The second set of models shows the seismic signatures of the Holsnøy, Cap de Creus, and Borborema shear zone for different noise levels (0%, 33%, 50%, 100%) (Fig. 5). Without noise, these models are identical to the intermediate frequency and illumination models described above (Figs. 3e, 4e and 5e). These models show clear seismic images of the shear zones, illuminating all reflections dipping below 45° (Fig. 6a–c). At 33% noise, it becomes difficult to identify some of the thinner parts of the shear zones against the background noise (Fig. 6d–f). At 50% noise, it is difficult to identify shear zones (Fig. 6g–i), because the amplitudes of the signal are on the same level as the noise, which is shown for comparison (Fig. 6j-l)

Table 3
Typical frequencies covered by seismic reflection surveys (e.g. Osagiede et al., 2014).

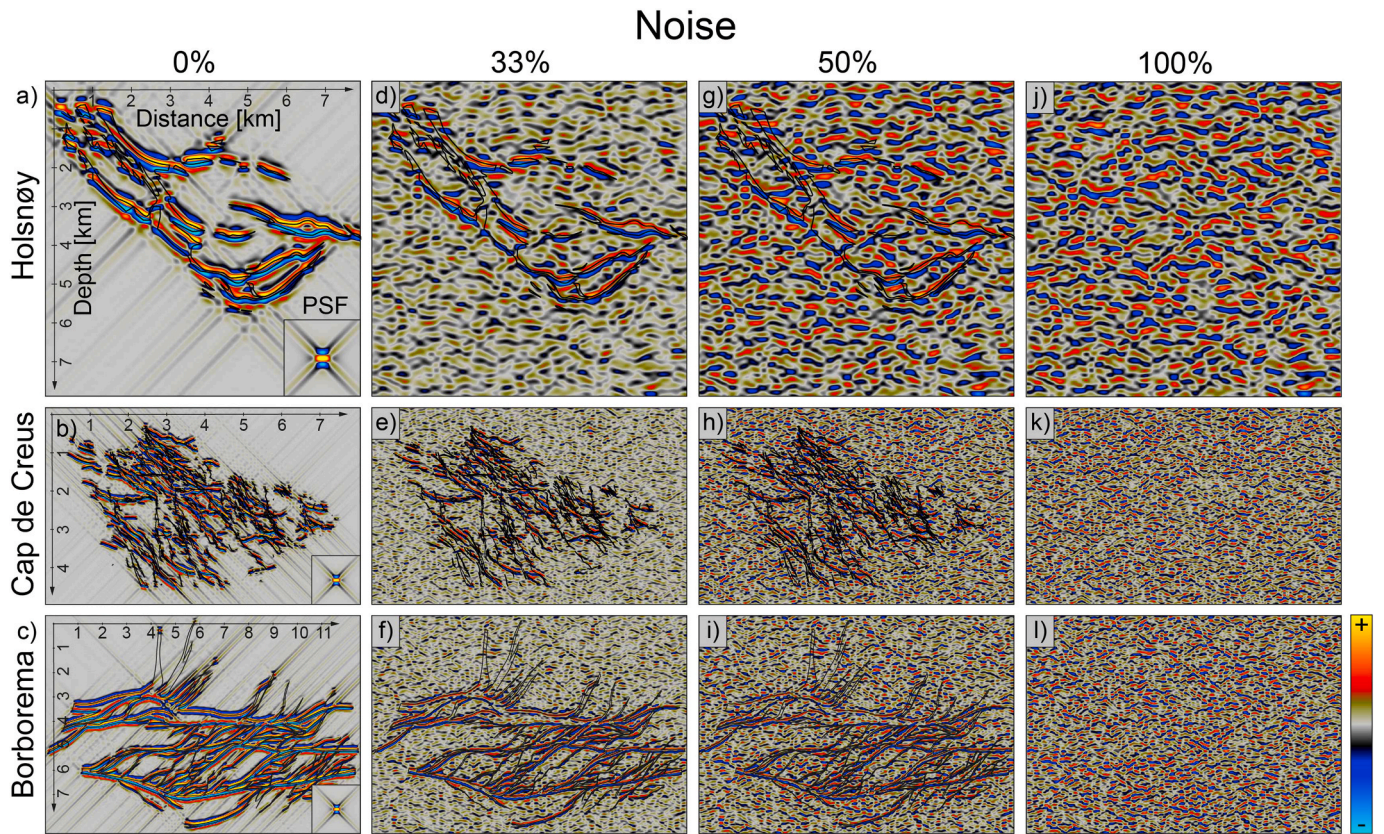| Location	Year	Dominant Frequency [Hz]			
		Shallow (1 s TWT)	Medium (2 s TWT)	Deep (4 s TWT)	Very deep (8 s TWT)
North Viking Graben, North Sea	1998	54	48	29	–
Egersund Basin, North Sea	2005	45	30	15	–
Northern North Sea	2017	50	35	20	10
Exmouth Basin, NW Australia	2000	–	49	21	–
Santos Basin, offshore Brazil	2001/02	35	25	–	–

Noise

Fig. 6. Seismic images of the Holsnøy (a,d,g,l), Cap de Creus (b,e,h,k) and Borborema shear zone (c,f,i,l) in cross-section for different levels of noise (0%, 33%, 50% and 100%). We use frequencies and illumination angles of 10 Hz and ≤45° for Holsnøy (Fig. 2e), 20 Hz and ≤45° for Cap de Creus (Figs. 3e), 10 Hz and ≤45° for Borborema (Fig. 4e); corresponding to intermediate imaging quality. The point-spread function (PSF) indicates the vertical and horizontal resolution of the seismic image. The seismic images correspond to zero-phase PSDM data. The colour bar is scaled to 50% of the maximum and minimum amplitudes. The black outline shows the shear zone geometry. To compare the extremely-large Borborema shear zone to seismic studies, it was necessary to scale its length and width down by a factor 50.

4.2. Geological effects

The third set of models explores how shear zone properties impact their seismic signature. These models show the seismic signatures of the Holsnøy, Cap de Creus, and Borborema shear zone networks for different aspect ratios (1:1, 1:2, 2:1) and dips (0°, 30°, 60°) (Figs. 7,8, 9). At 1:1 aspect ratio and zero dip, we obtain a good seismic image of the shear zone with all branches clearly visible (Figs. 7a, 8a and 9a). As we increase the dip to 30° (Figs. 7b, 8b and 9b) and 60° (Figs. 7c, 8c and 9c), we start to lose some of the steeper dipping reflections. At 1:2 aspect ratio, seismic reflections become closer and merge vertically (Figs. 7d–f, 8d-f, 9d-f). At 60° dip, it becomes difficult to identify the Holsnøy and Cap de Creus shear zone, as we only image a few sub-parallel reflections (Figs. 7f and 8f). The Borborema shear zones becomes virtually impossible to identity, as we lose almost all of the inclined reflection in the seismic image (Fig. 9f). At 2:1 aspect ratio, we image most strands of the shear zones, only losing some inclined reflections at 30° and 60° dip (Figs. 7g–i, 8g-i, 9g-i).

5. Discussion

5.1. Seismic indicators

Our models show that kilometre-scale shear zones mapped in the field can produce inclined seismic reflections similar to those observed in seismic reflection data from rifts and continental margins (Fig. 10a) (e.g. Fossen and Hurich, 2005; Fazlikhani et al., 2017). Subparallel, inclined reflections occur in almost all our models (Figs. 3, 4, 5, 6, 7,8, 9), given that shear zone dips do not exceed maximum illumination angles (e.g. Fig. 9).

This is consistent with previous 2-D and 3-D seismic studies, which interpret multiple, sub-parallel, inclined reflections as kilometre-scale shear zones (Fig. 10a) (e.g. Fossen and Hurich, 2005; Fazlikhani et al., 2017). This observations is, however, not sufficient for the interpretation of shear zones, as tilted layers or magmatic dykes can produce similar subparallel, inclined reflection packages (e.g. Phillips et al., 2016).

A second seismic indicator revealed by our models are cross-cutting seismic reflections. Most of our models show cross-cutting reflections resulting from intersections of different strands of these shear zone networks (Figs. 3, 4, 5, 6, 7,8, 9). This result is interesting, as cross-cutting reflections are typically associated with fluid contacts (e.g. Brown, 2011), gas hydrates (e.g. Berndt et al., 2004), silica diagenesis (e. g. Wrona et al., 2017), or magmatic intrusions (e.g. Magee et al., 2014), i.e. processes that can generate an impedance contrast that dissects existing stratigraphy. In contrast, our models highlight how cross-cutting reflections can originate from intersecting strands of shear zone networks (Fig. 10b), without requiring interaction with host stratigraphy. This is in line with previous studies, which upon re-examination, show several cross-cutting seismic reflections within shear zones (Fig. 10b) (e.g. Fazlikhani et al., 2017; Clerc et al., 2018). While fluid contacts, gas hydrates and silica diagenesis typically occur in the upper crust, seismic interpretations of the lower crust often require a distinction between shear zones and magmatic intrusions.

The third seismic indicator, which allows us to distinguish between shear zones and magmatic intrusions, are reflection junctions. More precisely, our models show that seismic reflections originating from shear zones consistently converge in the same direction towards the edge of the zone (Figs. 3, 4, 5, 6, 7,8, 9). These unidirectional reflection junctions are typical for shear zones observed in the field and seismic
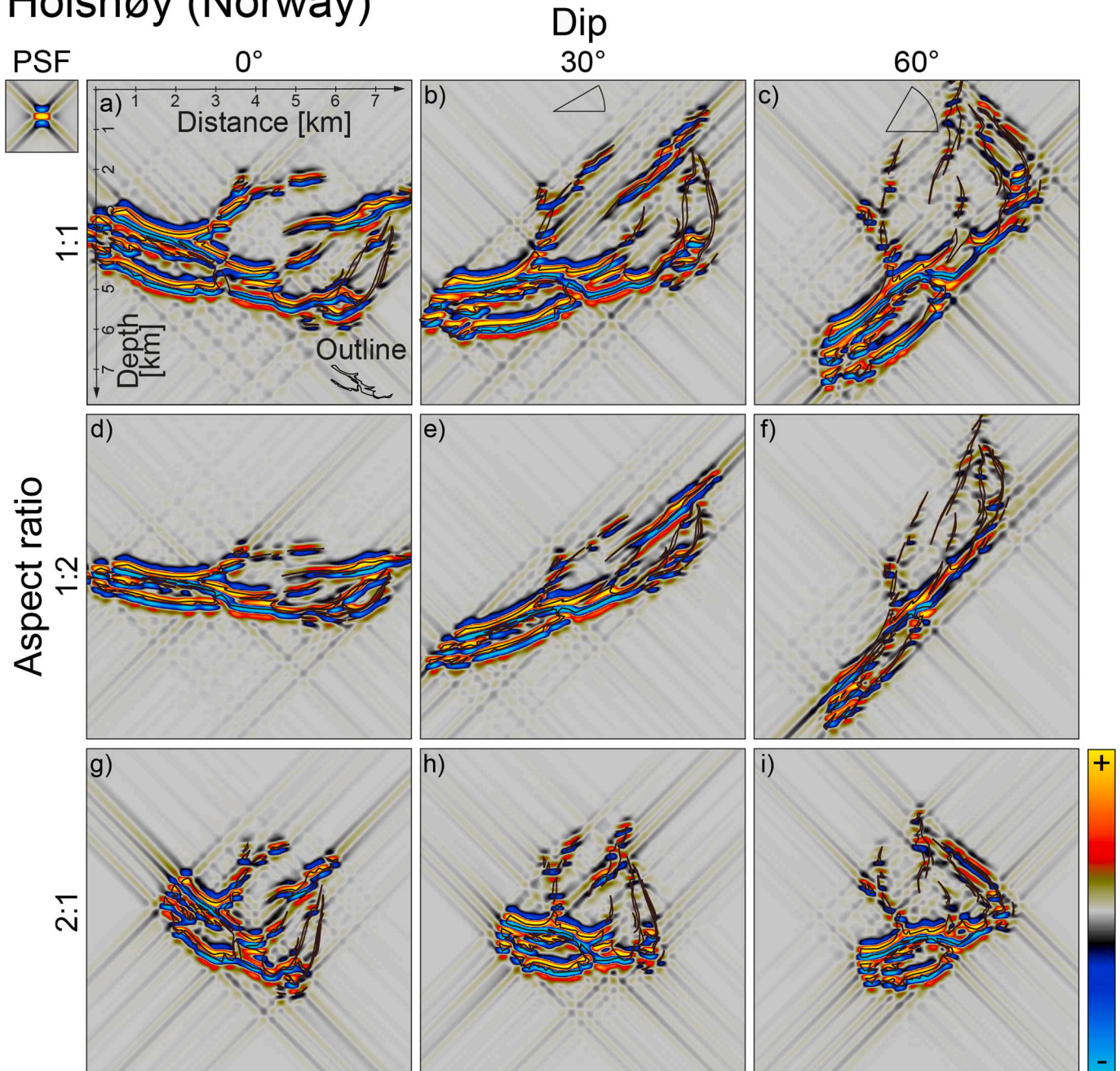
Fig. 7. Seismic images of the Holsnøy shear zone (Norway) in cross-section for different dips (0°, 30°, 60°) and aspect ratios (1:1, 1:2, 2:1) created with intermediate frequency (10 Hz) and illumination (≤45°). The point-spread function (PSF) indicates the vertical and horizontal resolution of the seismic image. The seismic images correspond to zero-phase PSDM data. The colour bar is scaled to 50% of the maximum and minimum amplitudes. The black outline shows the shear zone geometry.

reflection data (Fig. 10c). Moreover, they are in stark contrast to multidirectional reflection junctions observed in magmatic sill complexes (e.g. Magee et al., 2014; Eide et al., 2018; Wrona et al., 2019) allowing a clear distinction between shear zones and magmatic intrusions in seismic reflection data.

To summarize, we suggest to look for combinations of: (1) subparallel, inclined reflection packages; (2) cross-cutting reflections, and (3) unidirectional reflection junctions to identify shear zones in seismic reflection data (Fig. 10).

5.2. Kinematic indicators

In addition to identifying shear zones in seismic reflection data, we are often interested in their sense of movement. While shear zone orientation and/or geological history of the area can provide constraints on the sense of movement of a shear zone, we would prefer to obtain the kinematics directly from seismic reflection data. Our models suggest that seismic reflection orientation and curvature inside the shear zone indicate its sense of movement (Fig. 11). For instance, several strands of the dextral Holsnøy shear zone curve towards the edge of the shear zone forming an acute angle (Fig. 11a). This angle points consistently towards the direction of movement along the shear zone edge. A zoom-in of the
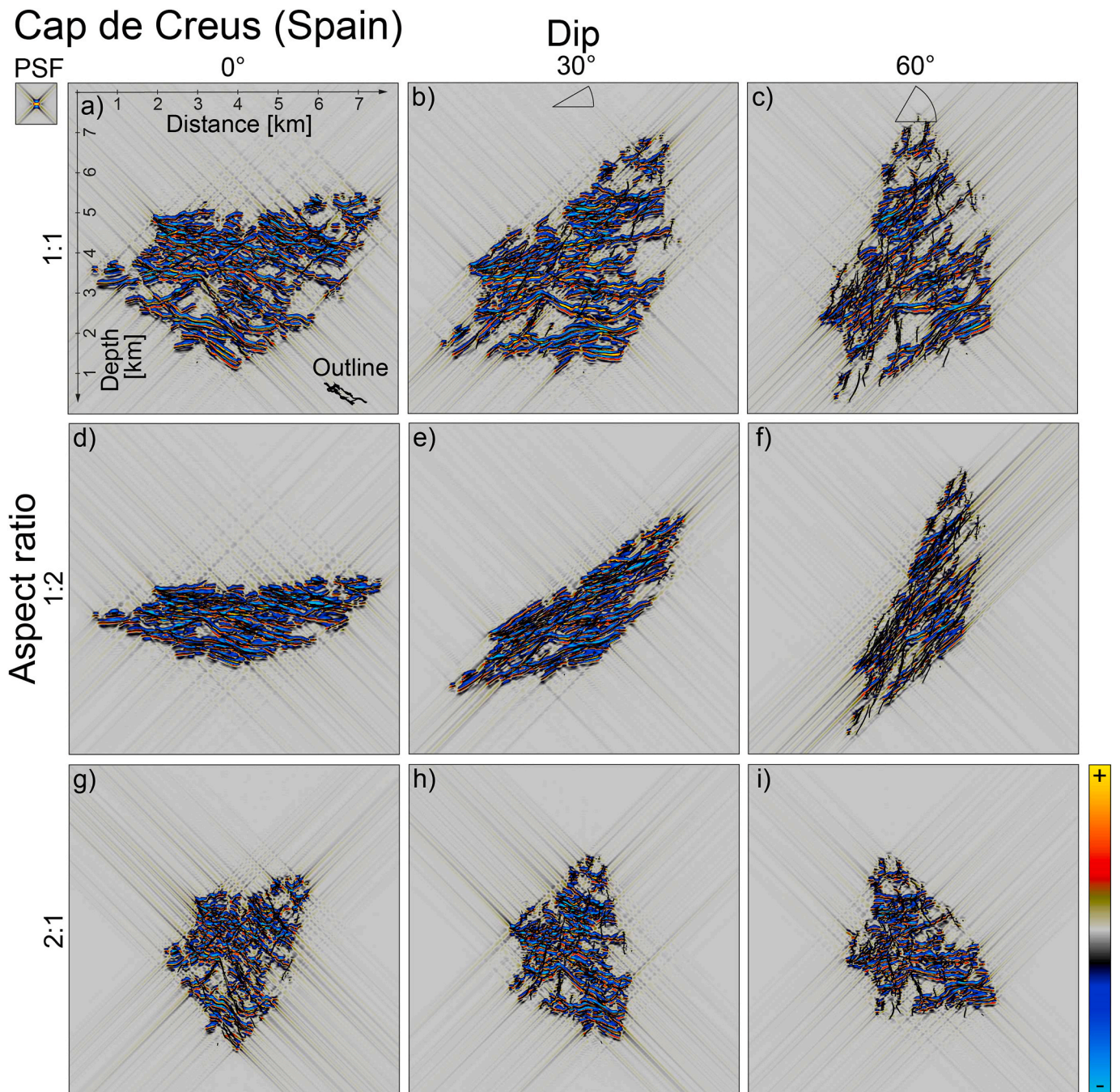
Fig. 8. Seismic images of the Cap de Creus shear zone (Spain) in cross-section for different dips (0°, 30°, 60°) and aspect ratios (1:1, 1:2, 2:1) created with intermediate frequency (20 Hz) and illumination (≤45°). The point-spread function (PSF) indicates the vertical and horizontal resolution of the seismic image. The seismic images correspond to zero-phase PSDM data. The colour bar is scaled to 50% of the maximum and minimum amplitudes. The black outline shows the shear zone geometry.

Borborema shear zone reveals the same pattern: seismic reflections curving towards the edge of the shear zone in the direction of movement (Fig. 11d). Our models show that this pattern can translate into seismic images of these shear zones at moderate frequencies (10 Hz), illumination angles (≤45°) and levels of noise (33%) (Fig. 11b,e). At lower frequencies, this pattern is probably more difficult to image (Figs. 2 and 4). The pattern is consistent with seismic observations from the Uruguayan continental margin (Clerc et al., 2015), which show this relationship between seismic reflection inside and at the edge of the shear zone (Fig. 11c,f). This gives us confidence that this simple geometric

relationship known from field observations (e.g. Ramsay, 1980) is a useful kinematic indicator for shear zone observed in in 2-D and 3-D seismic reflection data.

5.3. Hidden structures

While we often concentrate on the shear zones observable in our dataset, it is worth thinking about the ones that we are missing. For example, our models confirm our intuition that shear zones become very difficult to image at low frequencies (≤10 Hz), illumination (≤30°) and
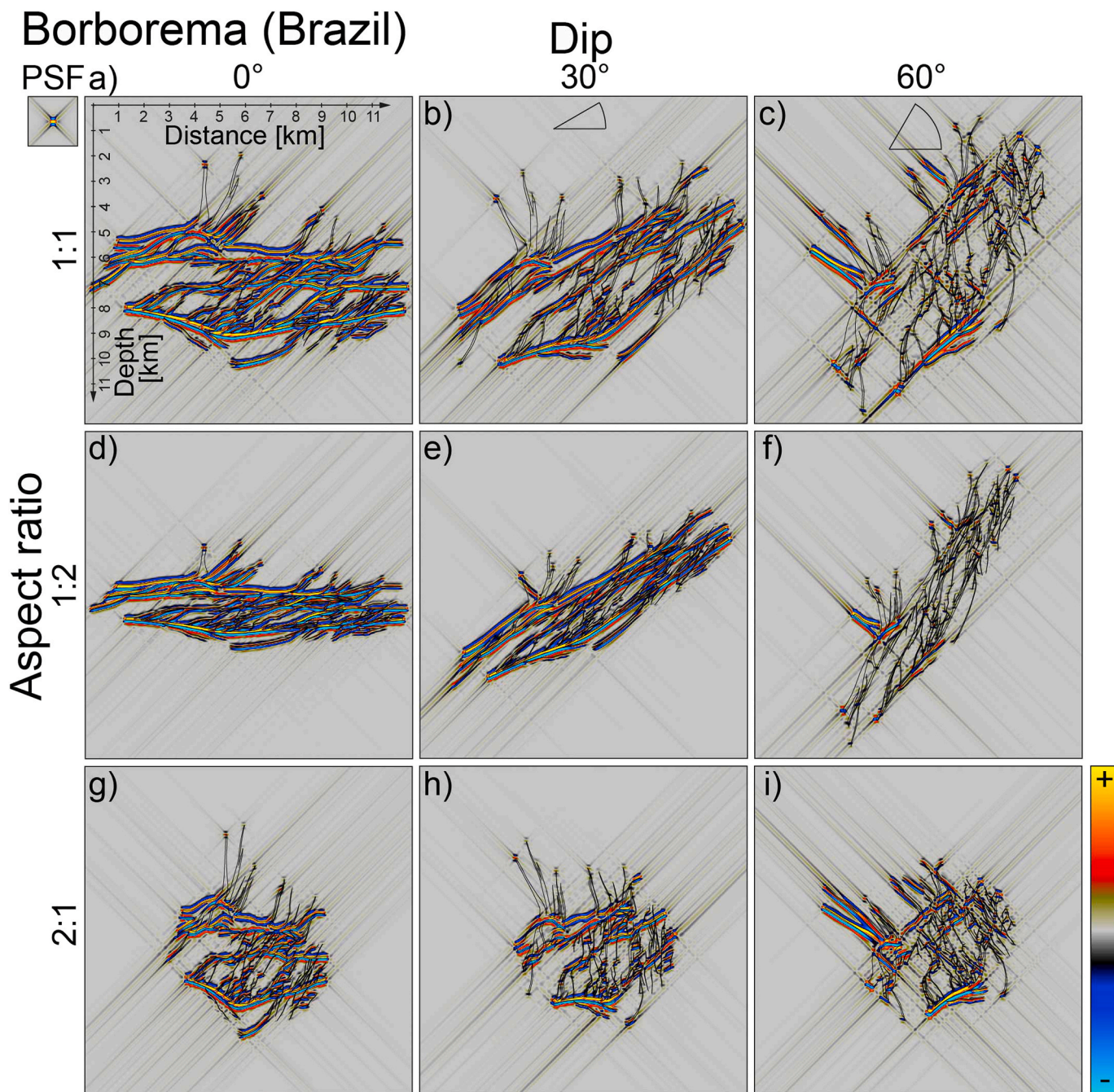
Fig. 9. Seismic images of the Borborema shear zone (Brazil) in cross-section for different dips (0°, 30°, 60°) and aspect ratios (1:1, 1:2, 2:1) created with intermediate frequency (10 Hz) and illumination (≤45°). The point-spread function (PSF) indicates the vertical and horizontal resolution of the seismic image. The seismic images correspond to zero-phase PSDM data. The colour bar is scaled to 50% of the maximum and minimum amplitudes. The black outline shows the shear zone geometry. To compare the extremely-large Borborema shear zone to seismic studies, it was necessary to scale its length and width down by a factor 50.
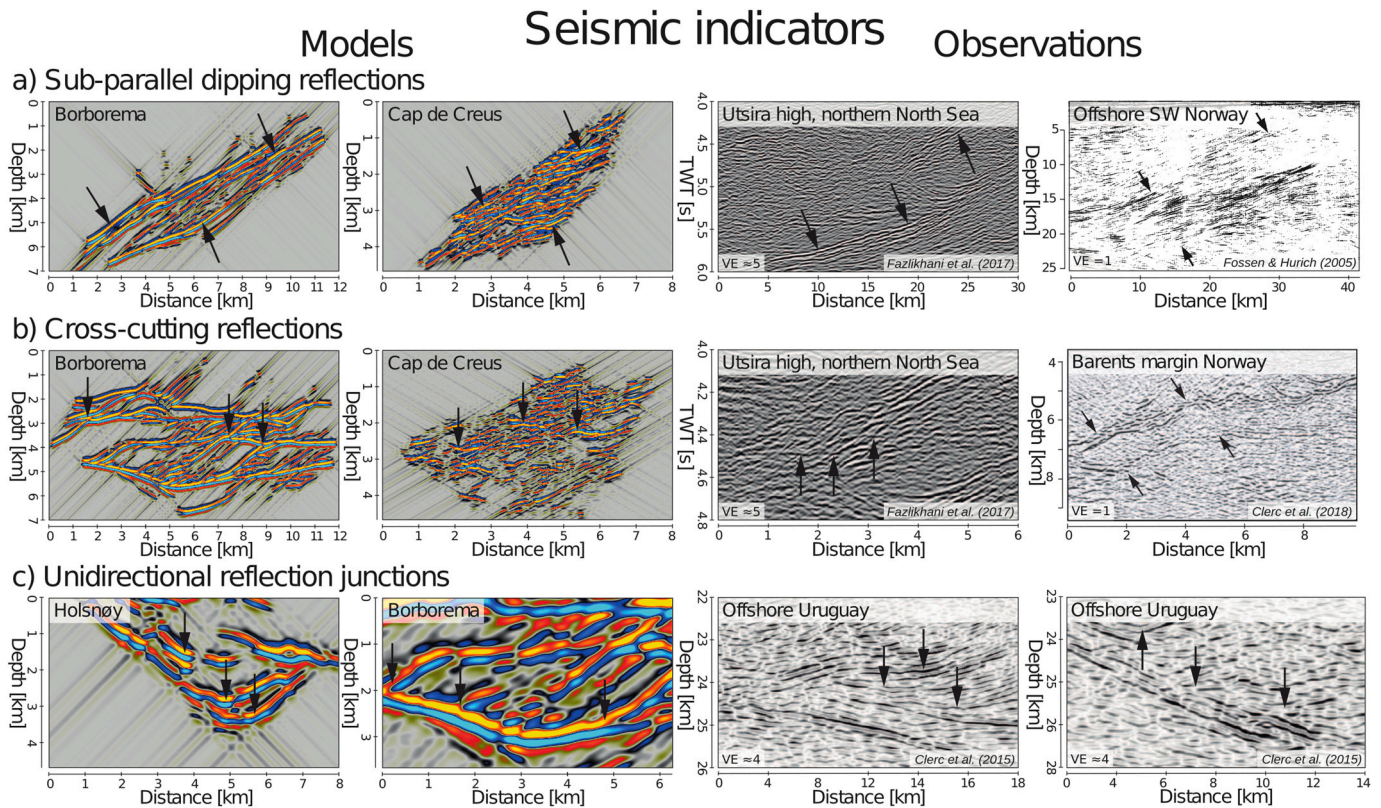
Fig. 10. Seismic indicators of crustal shear zones in our models in comparison to previous marine seismic reflection studies from offshore southern and northern Norway (Phillips et al., 2016; Fazlikhani et al., 2017; Lenhart et al., 2019) and Uruguay (Clerc et al., 2015). While our seismic images have no vertical exaggeration (VE), the seismic images from previous studies are vertically exaggerated (factor on the bottom left of images). Our first example showing sub-parallel dipping reflections from the Borborema shear zones was generated with a frequency of 10 Hz, ≤45° illumination, 30° dip and an aspect ratio of 1:2 (Fig. 8e). The second example showing the Cap de Creus shear zone was create with a frequency of 20 Hz, ≤45° illumination, 30° dip and an aspect ratio of 1:2 (Fig. 7e). Third example showing cross-cutting reflections of the Borborema shear zone was generated with a frequency of 10 Hz, ≤45° illumination, no dip and an 1:1 aspect ratio (Fig. 8a). The forth example from the Cap de Creus shear zone was generated with a frequency of 10 Hz, ≤30° illumination, the original dip and aspect ratio (Fig. 3f). The fifth example showing unidirectional reflection junctions of the Holsnøy shear zone was computed with a frequency of 10 Hz, ≤45° illumination, the original dip and aspect ratio (Fig. 2e) and the last example showing a zoom-in of the Borborema shear zone was generated with a frequency of 10 Hz, ≤45° illumination, no dip and an 1:1 aspect ratio (Fig. 8a).

high levels (50%) of noise (Figs. 3, 4, 5, 6). This is an important point to remember when estimating the total strain of a system, because large fractions of the strain might not be imaged due to limitations of our dataset. On the other side, we may also miss shear zones with certain geometries. Our models, for example, suggest that shear zones dipping steeper than the illumination of our survey are difficult to image (Figs. 7, 8, 9). This is particularly important in areas, where we would expect steeply inclined shear zones such as regions of strike-slip motion. Combining these results with the general trend that illumination decreases with depth, it is virtually impossible to image steeply inclined shear zones deep in the lower crust using conventional seismic reflection surveys.

5.4. Geological complexity

While our models are based on detailed geological mapping of large-scale shear zones (Fig. 1), it is not possible to include the full complexity observed in the field. For example, we built these models using only two rock types: shear zone and host rock, which are already difficult to constrain by physical measurements (see Table 2), yet in nature, these rocks are highly variable in terms of composition, metamorphic grade and degree of deformation (e.g. Austrheim et al., 1997; Neves and Mariano, 1999; Carreras, 2001). Including all these elements in our models would require accurate physical measurements of rocks sampled at high resolution over large areas. Even if we would have built our

models with such measurements, physical rock properties measured in the laboratory probably differ from those encountered in the subsurface, where pressures, temperatures, and pore fluids are different and change with time. A final feature that was not possible to include in these large-scale models due to their resolution (1 m), are microscopic structures, such as foliation, fractures, and veins.

5.5. Geophysical limitations

While our models produce 2-D seismic images comparable to those observed in continental rifts and margins (Figs. 10 and 11), it is not possible to simulate all geophysical effects with these models. For example, our models do not include seismic velocity anisotropies, which are expected to occur in shear zones (e.g. Godfrey et al., 2000; Wenning et al., 2018), but cannot be constrained given the size and complexity of these outcrop examples and the absence of in-situ physical property measurements. With regards to amplitudes, our models simulate perfect processing removing all effects of geometrical spreading, attenuation, and dispersion. In nature, these effects are expected to reduce the overall imaging quality. Finally, it is worth emphasizing that we, similar to most field- and seismic studies, approach a 3-D problem with 2-D models. While generating synthetic 3-D seismic reflection data is possible, it would require large-scale 3-D outcrop observations to generate these models.
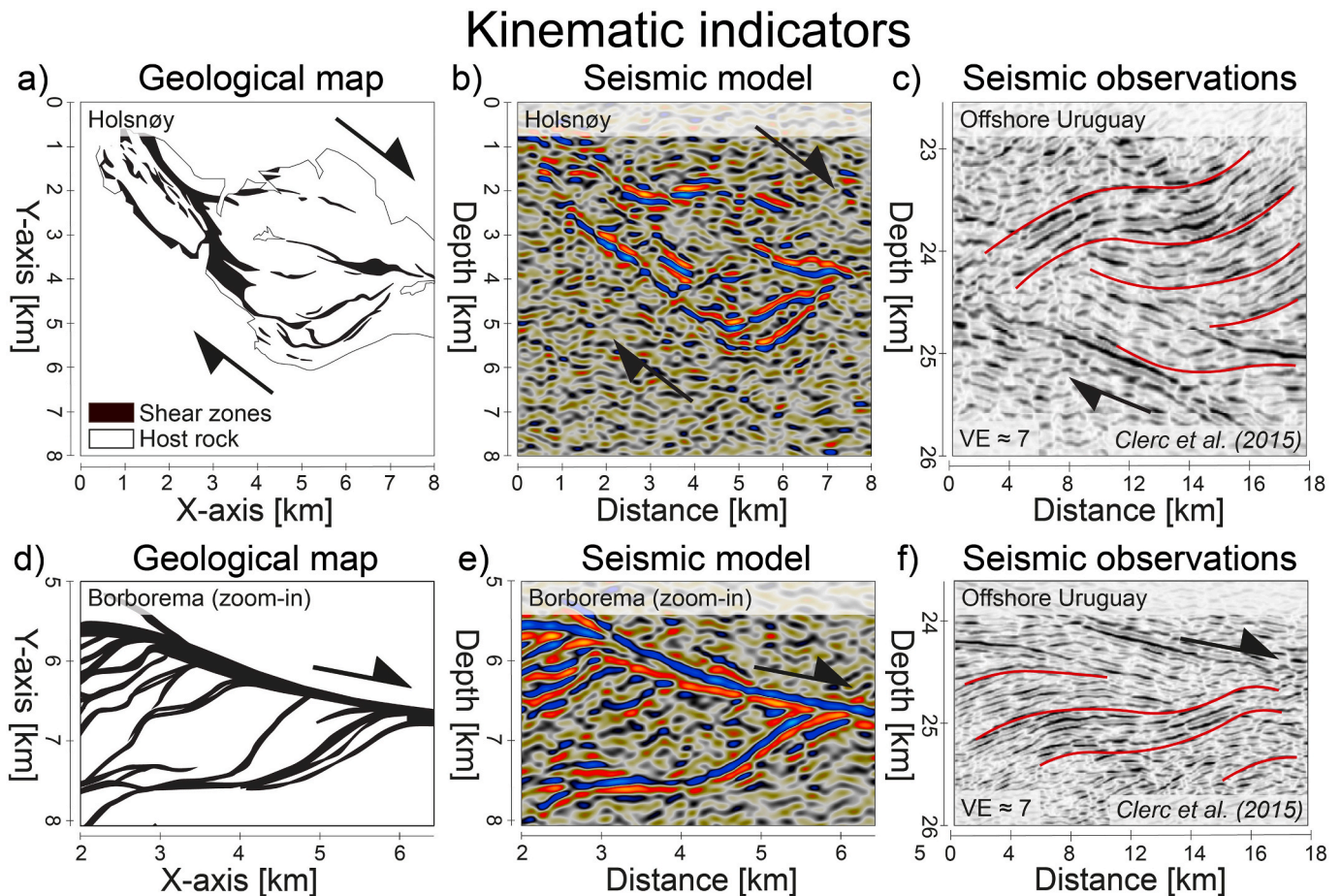
Fig. 11. Kinematic indicators showing the sense of movement of shear zones in geological maps, models and observations. a) Geological map of Holsnøy shear zone, Norway (Boundy et al., 1992; Austrheim et al., 1997), b) Seismic model of Holsnøy shear zone generated with a frequency of 10 Hz, ≤45° illumination, the original dip and aspect ratio (Fig. 5d), c) Seismic observations from lower crustal shear zone offshore Uruguay (Clerc et al., 2015), d) Geological map (zoom-in) of the Borborema shear zone network, Brazil (Neves and Mariano, 1999), e) Seismic model of the Borborema shear zone network created with a frequency of 10 Hz, ≤45° illumination, the original dip and aspect ratio (Fig. 5f), and f) Seismic observations from lower crustal shear zone offshore Uruguay (Clerc et al., 2015). Note that the curvature of the direction seismic reflections (red lines) at the shear zone margin indicates the sense of movement of the shear zone.

6. Conclusions

Simulating the 2-D seismic signature of three outcrop areas of shear zones (Holsnøy, Cap de Creus and Borborema) with point-spread-function based convolution modelling reveals three consistent characteristics: (1) multiple, sub-parallel, inclined reflections, (2) converging reflections, and (3) cross-cutting reflections. These features are clear in most cases, but become difficult to recognize when shear zones are dipping steeper than the illumination of the seismic survey or at high levels of noise (>50%). Moreover, we find that reflection curvature at the shear zone edge is a useful kinematic indicator, as seismic reflections forming an acute angle with the edge of the shear zone indicate the direction of movement of the shear zone. In spite of several simplifying assumptions, we believe that this work gives strong support to the general assumption that shear zones can be identified and their geometry can be mapped in seismic reflection data based on the characteristics listed above.

CRediT authorship contribution statement

T. Wrona: Conceptualization, Writing - original draft, Writing - review & editing, Visualization. **H. Fossen:** Conceptualization, Writing - review & editing, Supervision, Project administration, Funding acquisition. **I. Lecomte:** Conceptualization, Methodology, Software, Writing - review & editing, Visualization. **C.H. Eide:** Conceptualization, Methodology, Writing - review & editing. **R.L. Gawthorpe:** Conceptualization, Writing - review & editing, Supervision, Project administration, Funding acquisition.

References

Archanjo, C.J., Trindade, R.I.F., Bouchez, J.L., Ernesto, M., 2002. Granite fabrics and regional-scale strain partitioning in the Seridó belt (Borborema Province, NE Brazil). Tectonics 21. https://doi.org/10.1029/2000tc001269, 3-1-3–14.
Austrheim, H., 1987. Eclogitization of lower crustal granulites by fluid migration through shear zones. Earth Planet Sci. Lett. 81, 221–232. https://doi.org/10.1016/0012-821X(87)90158-0.

Austrheim, H., 1990. The granulite-eclogite facies transition: a comparison of experimental work and a natural occurrence in the Bergen Arcs, western Norway. Lithos 25, 163–169. https://doi.org/10.1016/0024-4937(90)90012-P.

Austrheim, H., Erambert, M., Engvik, A.K., 1997. Processing of crust in the root of the Caledonian continental collision zone: the role of eclogitization. Tectonophysics 273, 129–153. https://doi.org/10.1016/S0040-1951(96)00291-0.

Austrheim, H., Griffin, W.L., 1985. Shear deformation and eclogite formation within granulite-facies anorthosites of the Bergen Arcs, western Norway. Chem. Geol. 50, 267–281. https://doi.org/10.1016/0009-2541(85)90124-X.

Berndt, C., Bünz, S., Clayton, T., Mienert, J., Saunders, M., 2004. Seismic character of bottom simulating reflectors: examples from the mid-Norwegian margin. Mar. Petrol. Geol. 21, 723–733. https://doi.org/10.1016/j.marpetgeo.2004.02.003.

Bingen, B., Austrheim, H., Whitehouse, M.J., Davis, W.J., 2004. Trace element signature and U-Pb geochronology of eclogite-facies zircon, Bergen Arcs, Caledonides of W Norway. Contrib. Mineral. Petrol. 147, 671–683. https://doi.org/10.1007/s00410-004-0585-z.

Boundy, T.M., Fountain, D.M., Austrheim, H., 1992. Structural development and petrofabrics of eclogite facies shear zones, Bergen Arcs, western Norway: implications for deep crustal deformational processes. J. Metamorph. Geol. 10, 127–146. https://doi.org/10.1111/j.1525-1314.1992.tb00075.x.

Bourbié, T., Coussy, O., Zinszner, B., 1987. Acoustics of Porous Media. Editions Technip: Editions Technip, p. 334. https://books.google.ca/books/about/Acoustics_of_porous_media.html?id=2ozNKWDUXU4C&hl=en.

Brown, A.R., 2011. Interpretation of Seismic Data. The American Association of Petroleum Geologists and the Society of Exploration Geophysicists, pp. 1–18. https://doi.org/10.1190/1.9781560802884.

Carreras, J., 2001. Zooming on northern Cap de Creus shear zones. J. Struct. Geol. 23, 1457–1486. https://doi.org/10.1016/S0191-8141(01)00011-6.

de Castro, D.L., Bezerra, F.H.R., Castelo Branco, R.M.G., 2008. Geophysical evidence of crustal-heterogeneity control of fault growth in the Neocomian Iguatu basin, NE Brazil. J. S. Am. Earth Sci. 26, 271–285. https://doi.org/10.1016/j.jsames.2008.07.002.

de Castro, D.L., Bezerra, F.H.R., Sousa, M.O.L., Fuck, R.A., 2012. Influence of Neoproterozoic tectonic fabric on the origin of the Potiguar Basin, northeastern Brazil and its links with West Africa based on gravity and magnetic data. J. Geodyn. 54, 29–42. https://doi.org/10.1016/j.jog.2011.09.002.

Clerc, C., Jolivet, L., Ringenbach, J.C., 2015. Ductile extensional shear zones in the lower crust of a passive margin. Earth Planet Sci. Lett. 431, 1–7. https://doi.org/10.1016/j.epsl.2015.08.038.

Clerc, C., Ringenbach, J.C., Jolivet, L., Ballard, J.F., 2018. Rifted margins: ductile deformation, boudinage, continentward-dipping normal faults and the role of the weak lower crust. Gondwana Res. 53, 20–40. https://doi.org/10.1016/j.gr.2017.04.030.

Duretz, T., Schmalholz, S.M., Podladchikov, Y.Y., Yuen, D.A., 2014. Physics-controlled thickness of shear zones caused by viscous heating: implications for crustal shear localization. Geophys. Res. Lett. 41, 4904–4911. https://doi.org/10.1002/2014GL060438.

Eide, C.H., Schofield, N., Lecomte, I., Buckley, S.J., Howell, J.A., 2018. Seismic interpretation of sill complexes in sedimentary basins: implications for the sub-sill imaging problem. J. Geol. Soc. 175, 193–209. https://doi.org/10.1144/jgs2017-096.

Fazlikhani, H., Fossen, H., Gawthorpe, R.L., Faleide, J.I., Bell, R.E., 2017. Basement structure and its influence on the structural configuration of the northern North Sea rift. Tectonics 36, 1151–1177. https://doi.org/10.1002/2017TC004514.

Fossen, H., 2010. Extensional Tectonics in the North Atlantic Caledonides: A Regional View, vol. 335. Geological Society Special Publication, pp. 767–793. https://doi.org/10.1144/SP335.31.

Fossen, H., 1993. Structural evolution of the Bergsdalen Nappes, Southwest Norway. Bull. - Norges Geol. Undersokelse 424, 23–49.

Fossen, H., Cavalcante, G.C.G., 2017. Shear zones – a review. Earth Sci. Rev. 171, 434–455. https://doi.org/10.1016/j.earscirev.2017.05.002.

Fossen, H., Hurich, C.A., 2005. The Hardangerfjord shear zone in SW Norway and the North Sea: a large-scale low-angle shear zone in the caledonian crust. J. Geol. Soc. 162, 675–687. https://doi.org/10.1144/0016-764904-136.

Foster, D.A., Goscombe, B.D., Gray, D.R., 2009. Rapid exhumation of deep crust in an obliquely convergent orogen: the kaoko belt of the damara orogen. Tectonics 28. https://doi.org/10.1029/2008TC002317.

Ganade de Araujo, C.E., Weinberg, R.F., Cordani, U.G., 2014. Extruding the Borborema Province (NE-Brazil): a two-stage Neoproterozoic collision process. Terra. Nova 26, 157–168. https://doi.org/10.1111/ter.12084.

Gapais, D., Bale, P., Choukroune, P., Cobbold, P.R., Mahjoub, Y., Marquer, D., 1987. Bulk kinematics from shear zone patterns: some field examples. J. Struct. Geol. 9, 635–646. https://doi.org/10.1016/0191-8141(87)90148-9.

Godfrey, N.J., Beaudoin, B.C., Klemperer, S.L., Levander, A., Luetgert, J., Meltzer, A., Mooney, W., Tréhu, A., 1997. Ophiolitic basement to the Great Valley forearc basin, California, from seismic and gravity data: implications for crustal growth at the North American continental margin. Bull. Geol. Soc. Am. 109, 1536–1562. https://doi.org/10.1130/0016-7606(1997)109<1536:OBTTGV>2.3.CO;2.

Godfrey, N.J., Christensen, N.I., Okaya, D.A., 2000. Anisotropy of schists: contribution of crustal anisotropy to active source seismic experiments and shear wave splitting observations. J. Geophys. Res.: Solid Earth 105, 27991–28007. https://doi.org/10.1029/2000jb900286.

Gontijo-Pascutti, A., Bezerra, F.H.R., Terra, E. La, Almeida, J.C.H., 2010. Brittle reactivation of mylonitic fabric and the origin of the Cenozoic Rio Santana Graben, southeastern Brazil. J. S. Am. Earth Sci. 29, 522–536. https://doi.org/10.1016/j.jsames.2009.06.007.

Goscombe, B.D., Gray, D.R., 2008. Structure and strain variation at mid-crustal levels in a transpressional orogen: a review of Kaoko Belt structure and the character of West Gondwana amalgamation and dispersal. Gondwana Res. 13, 45–85. https://doi.org/10.1016/j.gr.2007.07.002.

Goscombe, B., Hand, M., Gray, D., 2003. Structure of the Kaoko Belt, Namibia: progressive evolution of a classic transpressional orogen. J. Struct. Geol. 25, 1049–1081. https://doi.org/10.1016/S0191-8141(02)00150-5.

Jafarian, E., de Jong, K., Kleipool, L.M., Scheibner, C., Blomeier, D.P.G., Reijmer, J.J.G., 2018. Synthetic seismic model of a Permian biosiliceous carbonate – carbonate depositional system (Spitsbergen, Svalbard Archipelago). Mar. Petrol. Geol. 92, 78–93. https://doi.org/10.1016/j.marpetgeo.2018.01.034.

Johnston, S., Hacker, B.R., Ducea, M.N., 2007. Exhumation of ultrahigh-pressure rocks beneath the Hornelen segment of the Nordfjord-Sogn detachment zone, western Norway. Bull. Geol. Soc. Am. 119, 1232–1248. https://doi.org/10.1130/B26172.1.

Kirkpatrick, J.D., Bezerra, F.H.R., Shipton, Z.K., Do Nascimento, A.F., Pytharouli, S.I., Lunn, R.J., Soden, A.M., 2013. Scale-dependent influence of pre-existing basement shear zones on rift faulting: a case study from NE Brazil. J. Geol. Soc. 170, 237–247. https://doi.org/10.1144/jgs2012-043.

Kiss, D., Podladchikov, Y., Duretz, T., Schmalholz, S.M., 2019. Spontaneous generation of ductile shear zones by thermal softening: localization criterion, 1D to 3D modelling and application to the lithosphere. Earth Planet Sci. Lett. 519, 284–296. https://doi.org/10.1016/j.epsl.2019.05.026.

Klepeis, K.A., Daczko, N.R., Clarke, G.L., 1999. Kinematic vorticity and tectonic significance of superposed mylonites in a major lower crustal shear zone, northern Fiordland, New Zealand. J. Struct. Geol. 21, 1385–1405. https://doi.org/10.1016/S0191-8141(99)00091-7.

Koehn, D., Link, K., Sachau, T., Passchier, C.W., Aanyu, K., Spikings, A., Harbinson, R., 2016. The Rwenzori Mountains, a Palaeoproterozoic crustal shear belt crossing the Albertine rift system. Int. J. Earth Sci. 105, 1693–1705. https://doi.org/10.1007/s00531-015-1167-1.

Lecomte, I., 2008. Resolution and illumination analyses in PSDM: a ray-based approach. Lead. Edge 27, 650–663. https://doi.org/10.1190/1.2919584.

Lecomte, I., Lavadera, P.L., Anell, I., Buckley, S.J., Schmid, D.W., Heeremans, M., 2015. Ray-based seismic modeling of geologic models: understanding and analyzing seismic images efficiently. Interpretation 3, SAC71–SAC89. https://doi.org/10.1190/INT-2015-0061.1.

Lecomte, I., Lavadera, P.L., Botter, C., Anell, I., Buckley, S.J., Eide, C.H., Grippa, A., Mascolo, V., Kjoberg, S., 2016. 2(3)D convolution modelling of complex geological targets beyond – 1D convolution. First Break 34, 99–107. http://fb.eage.org/publication/content?id=84451.

Lenhart, A., Jackson, C.A.L., Bell, R.E., Duffy, O.B., Gawthorpe, R.L., Fossen, H., 2019. Structural architecture and composition of crystalline basement offshore west Norway. Lithosphere 11, 273–293. https://doi.org/10.1130/L668.1.

Magee, C., Jackson, C.A.L., Schofield, N., 2014. Diachronous sub-volcanic intrusion along deep-water margins: insights from the Irish Rockall Basin. Basin Res. 26, 85–105. https://doi.org/10.1111/bre.12044.

Mainprice, D., Casey, M., 1990. The calculated seismic properties of quartz mylonites with typical fabrics: relationship to kinematics and temperature. Geophys. J. Int. 103, 599–608. https://doi.org/10.1111/j.1365-246X.1990.tb05674.x.

Manghnani, M.H., Ramananantoandro, R., Clark, S.P., 1974. Compressional and shear wave velocities in granulite facies rocks and eclogites to 10 kbar. J. Geophys. Res. 79, 5427–5446. https://doi.org/10.1029/jb079i035p05427.

Milnes, A.G., Wennberg, O.P., Skår, Koestler, A.G., 1997. Contraction, Extension and Timing in the South Norwegian Caledonides: the Sognefjord Transect, vol. 121. Geological Society Special Publication, pp. 123–148. https://doi.org/10.1144/GSL.SP.1997.121.01.06.

Neves, S.P., Mariano, G., 1999. Assessing the tectonic significance of a large-scale transcurrent shear zone system: the Pernambuco lineament, northeastern Brazil. J. Struct. Geol. 21, 1369–1383. https://doi.org/10.1016/S0191-8141(99)00097-8.

Norton, M.G., 1986. Late Caledonide Extension in western Norway: a response to extreme crustal thickening. Tectonics 5, 195–204. https://doi.org/10.1029/TC005i002p00195.

Osagiede, E.E., Duffy, O.B., Jackson, C.A.L., Wrona, T., 2014. Quantifying the growth history of seismically imaged normal faults. J. Struct. Geol. 66, 382–399. https://doi.org/10.1016/j.jsg.2014.05.021.

Passchier, C.W., Trouw, R.A.J., Ribeiro, A., Paciullo, F.V.P., 2002. Tectonic evolution of the southern Kaoko belt, Namibia. J. Afr. Earth Sci. 35, 61–75. https://doi.org/10.1016/S0899-5362(02)00030-1.

Phillips, T.B., Jackson, C.A.L., Bell, R.E., Duffy, O.B., Fossen, H., 2016. Reactivation of intrabasement structures during rifting: a case study from offshore southern Norway. J. Struct. Geol. 91, 54–73. https://doi.org/10.1016/j.jsg.2016.08.008.

Raimbourg, H., Jolivet, L., Labrousse, L., Leroy, Y., Avigad, D., 2005. Kinematics of syneclogite deformation in the Bergen Arcs, Norway: implications for exhumation mechanisms. Geol. Soc. Spec. Publ. 243, 175–192. https://doi.org/10.1144/GSL.SP.2005.243.01.13.

Ramsay, J.G., 1980. Shear zone geometry: a review. J. Struct. Geol. 2, 83–99. https://doi.org/10.1016/0191-8141(80)90038-3.

Salomon, E., Koehn, D., Passchier, C., 2015. Brittle reactivation of ductile shear zones in NW Namibia in relation to South Atlantic rifting. Tectonics 34, 70–85. https://doi.org/10.1002/2014TC003728.

Sheriff, R.E., Geldart, L.P., 1995. Explor. Seismol. https://doi.org/10.1017/cbo9781139168359.

Snyder, D.B., Kjarsgaard, B.A., 2013. Mantle Roots of Major Precambrian Shear Zones Inferred from Structure of the Great Slave Lake Shear Zone, Northwest Canada, vol. 5, pp. 539–546. https://doi.org/10.1130/L299.1. Lithosphere.

Vauchez, A., Tommasi, A., Mainprice, D., 2012. Faults (shear zones) in the Earth's mantle. Tectonophysics 558–559, 1–27. https://doi.org/10.1016/j.tecto.2012.06.006.

Wennberg, O.P., Milnes, A.G., Winsvold, I., 1998. The northern Bergen Arc shear zone-an oblique-lateral ramp in the Devonian extensional detachment system of western Norway. Nor. Geol. Tidsskr. 78, 169–184. ISSN 0029-196X.

Wenning, Q.C., Madonna, C., De Haller, A., Burg, J.P., 2018. Permeability and seismic velocity anisotropy across a ductile-brittle fault zone in crystalline rock. Solid Earth 9, 683–698. https://doi.org/10.5194/se-9-683-2018.

Wrona, T., Jackson, C.A.L., Huuse, M., Taylor, K.G., 2017. Silica diagenesis in Cenozoic mudstones of the North Viking Graben: physical properties and basin modelling. Basin Res. 29, 556–575. https://doi.org/10.1111/bre.12168.

Wrona, T., Magee, C., Fossen, H., Gawthorpe, R.L., Bell, R.E., Jackson, C.A.L., Faleide, J. I., 2019. 3-D seismic images of an extensive igneous sill in the lower crust. Geology 47, 729–733. https://doi.org/10.1130/G46150.1.

Younes, A.I., McClay, K., 2002. Development of accommodation zones in the gulf of Suez-Red Sea rift, Egypt. AAPG (Am. Assoc. Pet. Geol.) Bull. 86, 1003–1026. https://doi.org/10.1306/61eedc10-173e-11d7-8645000102c1865d.